Int. J. Electrochem. Sci., 14 **(2019)** 7695 – 7702, doi: 10.20964/2019.08.63

International Journal of
ELECTROCHEMICAL
SCIENCE
www.electrochemsci.org

Short Communication

Enhanced Electrochemical Properties of Lu-doped $BaCeO_3$ and KCl-NaCl Composite as Electrolyte for Intermediate Temperature Solid Oxide Fuel Cells

Yan Han, Ruifeng Du, Chang Wang, Hongbin Zhai, Fufang Wu[*], *Hongtao Wang*[*]

[1] School of Chemical and Material Engineering, Fuyang Normal University; Anhui Provincial Key Laboratory for Degradation and Monitoring of Pollution of the Environment, Fuyang 236037, China
[2] Guangdong Provincial Key Lab of Nano-Micro Materials Research, School of Chemical Biology and Biotechnology, Peking University Shenzhen Graduate School, Shenzhen 518055, China
[*]E-mail: hwang@fync.edu.cn, wff05001@fync.edu.cn

Received: 7 April 2019 / *Accepted:* 24 May 2019 / *Published:* 30 June 2019

In this study, $BaCe_{0.9}Lu_{0.1}O_{3-\alpha}$ was prepared by the sol-gel method with cerium nitrate, lutetium oxide and barium acetate as raw materials and $BaCe_{0.9}Lu_{0.1}O_{3-\alpha}$-NaCl-KCl composite electrolyte was also synthesized using $BaCe_{0.9}Lu_{0.1}O_{3-\alpha}$ combined with sodium and potassium chloride. The samples were characterized by X-ray diffraction (XRD), scanning electron microscopy (SEM) and thermal analyser. TGA-DSC plots indicated that a perovskite-type structure was formed above 1040 °C. The highest conductivities of $BaCe_{0.9}Lu_{0.1}O_{3-\alpha}$ and $BaCe_{0.9}Lu_{0.1}O_{3-\alpha}$-NaCl-KCl were 9.5×10^{-2} $S\cdot cm^{-1}$ and 2.8×10^{-1} $S\cdot cm^{-1}$ at 700 °C, respectively. The highest power density of $BaCe_{0.9}Lu_{0.1}O_{3-\alpha}$-NaCl-KCl was 146 $mW\cdot cm^{-2}$ at 700 °C.

Keywords: Defects; Hydrogen; Electrolytes; Fuel cell; Conductivity; Composite

1. INTRODUCTION

Solid oxide fuel cells (SOFCs) are considered to be promising green energy technologies due to their fuel elasticity, high durability and energy conversion efficiency etc. [1-6]. SOFCs can be roughly divided into two categories, oxide and protonic ions, according to their conductive mechanism. The proton-conducting SOFC can operate at lower temperatures, thus widening the choice of materials for cells and auxiliary components [7-10]. $BaCeO_3$-based perovskites exhibit higher conductivity than Y_2O_3 stabilized ZrO_2 (YSZ) in the intermediate temperature range [11-20]. $BaCeO_3$-based oxides are usually prepared by traditional solid-state reaction (SSR). The SSR method may lead to crystal growth due to long calcination time, however, it hinders the formation of compact ceramics. A liquid phase

reaction method, such as sol-gel, microemulsion and citrate-nitrate combustion method, can obtain better homogeneity and reactivity, so that the samples can have compact particles with smaller size at lower sintering temperature.

In the 1990s, it was reported that adding inorganic materials to a solid electrolyte can effectively improve its conductivity [21-25]. Composite electrolytes have many advantages, such as high energy density, less pollution and flexible design size etc. They have been extensively studied for intermediate temperature solid oxide fuel cells. Liu et al. reported that $BaCe_{0.7}In_{0.3}O_{3-\delta}$–$Gd_{0.1}Ce_{0.9}O_{2-\delta}$ composite electrolytes with various weight ratios exhibited high mixed protonic and oxygen ionic conductivities [21]. Marques et al. found that the $Ce_{1.9}Gd_{0.1}O_{1.95}$-Li_2CO_3-Na_2CO_3 composite electrolytes had excellent long-term stability under various atmospheres [23]. Our latest research showed that $SrCeO_3$-based electrolyte-NaCl~KCl composite electrolytes had excellent medium temperature fuel cell performances [26-27]. The Lu^{3+} ionic radius is close to that of Ce^{4+} and there is little study about medium temperature ionic conduction of $BaCeO_3$-based oxides- NaCl~KCl composite electrolytes.

Therefore, in this study, $BaCe_{0.9}Lu_{0.1}O_{3-\alpha}$ was prepared by the sol-gel method with cerium nitrate, lutetium oxide and barium acetate as raw materials and $BaCe_{0.9}Lu_{0.1}O_{3-\alpha}$-NaCl-KCl composite electrolyte was also synthesized using $BaCe_{0.9}Lu_{0.1}O_{3-\alpha}$ combined with sodium and potassium chloride. The samples were characterized by X-ray diffraction (XRD), scanning electron microscopy (SEM) and thermal analyser. The medium temperature ionic conductions of the samples were also studied using an electrochemical workstation.

2. EXPERIMENTAL

$BaCe_{0.9}Lu_{0.1}O_{3-\alpha}$ was prepared by the sol-gel method with cerium nitrate, lutetium oxide and barium acetate as raw materials. 0.9948 g of lutetium oxide, 12.771g of barium acetate and 24.6699g of cerium nitrate were weighed by analytical balance. Lu_2O_3 was added into nitric acid to dissolve it. Barium acetate and cerium nitrate were dissolved with distilled water (150 ml). 19.213g of citric acid was added into the above solution. The *p*H was adjusted to 8.0 with ammonia. The solution was continuously stirred until it was as viscous as honey and put into a vacuum drying chamber at 120 °C for one day [28-30]. The ashed mixtures were sintered to obtain $BaCe_{0.9}Lu_{0.1}O_{3-\alpha}$ in a high temperature box furnace at 1250 ℃ and 1550 ℃ for 5 h, respectively.

$BaCe_{0.9}Lu_{0.1}O_{3-\alpha}$-NaCl-KCl composite electrolyte was also synthesized using $BaCe_{0.9}Lu_{0.1}O_{3-\alpha}$ combined with sodium and potassium chloride. $BaCe_{0.9}Lu_{0.1}O_{3-\alpha}$ and NaCl-KCl (1:1 mole ratio) were mixed at an 8:2 weight ratio. The mixtures were ground uniformly and screened with 200 mesh, then, pressed at 200 MPa and placed in a muffle furnace at 750 °C for 2 h to obtain $BaCe_{0.9}Lu_{0.1}O_{3-\alpha}$-NaCl-KCl.

The thermal analyser (TGA-DSC, Universal V 3.7A, TA Instruments, New Castle, DE, USA) was used before and after ashing measurement of $BaCe_{0.9}Lu_{0.1}O_{3-\alpha}$ gel. The XRD spectra of the two samples were obtained by an X-ray diffraction (XRD, X'pert Pro MPD, Holland's company, Amsterdam, Netherlands) to determine the structure and composition. Scanning electron microscopy

(SEM, S-4700, Hitachi, Tokyo, Japan) was used to observe the morphologies of the external and cross-sectional surfaces of $BaCe_{0.9}Lu_{0.1}O_{3-\alpha}$ and $BaCe_{0.9}Lu_{0.1}O_{3-\alpha}$-NaCl-KCl.

For AC impedance measurements, the prepared $BaCe_{0.9}Lu_{0.1}O_{3-\alpha}$ and $BaCe_{0.9}Lu_{0.1}O_{3-\alpha}$- NaCl-KCl were polished with sandpaper. The thicknesses of the samples were 1.0-1.1 mm. Both electrode sides were painted with silver-palladium paste and coated with silver mesh as collectors. The AC impedance was studied using the CHI660E series electrochemical workstation from 1 Hz to 100 KHz in dry nitrogen at 400–700 °C. In order to measure the fuel cell performances of the samples, oxygen and hydrogen were injected into the upper and lower gas chambers at 700 °C.

3. RESULTS AND DISCUSSION

TGA-DSC plots of $BaCe_{0.9}Lu_{0.1}O_{3-\alpha}$ gel was made before and after ashing measurement. In Fig. 1(a), the weight loss is about 34% from room temperature to 310 °C, and there is a broad endothermic peak, which is mainly due to the decomposition of citric acid. The $BaCe_{0.9}Lu_{0.1}O_{3-\alpha}$ has a sharp exothermic peak between 580 °C and 590 °C, which is mainly due to the decomposition of nitrate. There is almost no change in weight and heat flow after 1040 °C, which indicates that a perovskite-type structure is formed [31-32]. From Fig. 1(b), the weight loss after 800 °C is due to incomplete decomposition of residual organic matter during ashing measurement. The XRD patterns of $BaCe_{0.9}Lu_{0.1}O_{3-\alpha}$ and $BaCe_{0.9}Lu_{0.1}O_{3-\alpha}$-NaCl-KCl are shown in Fig. 2. The XRD pattern of the sintered $BaCe_{0.9}Lu_{0.1}O_{3-\alpha}$ shows it is orthorhombic $BaCeO_3$ phase. From the XRD analysis of $BaCe_{0.9}Lu_{0.1}O_{3-\alpha}$-NaCl-KCl, the diffraction peaks of the sample are consistent with that of $BaCe_{0.9}Lu_{0.1}O_{3-\alpha}$. In addition, there are other small diffraction peaks in the image, which are detected to be NaCl and KCl. However, the weak diffraction peaks indicate that NaCl and KCl exist in an amorphous state besides a crystalline phase [28].

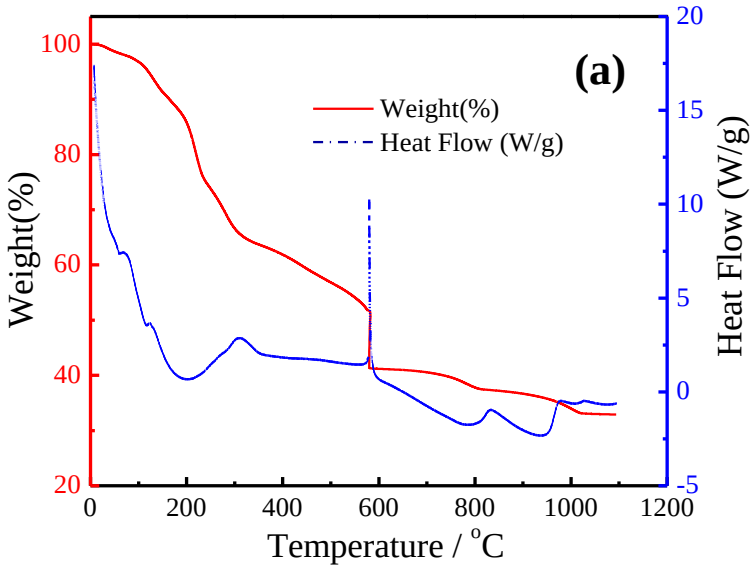

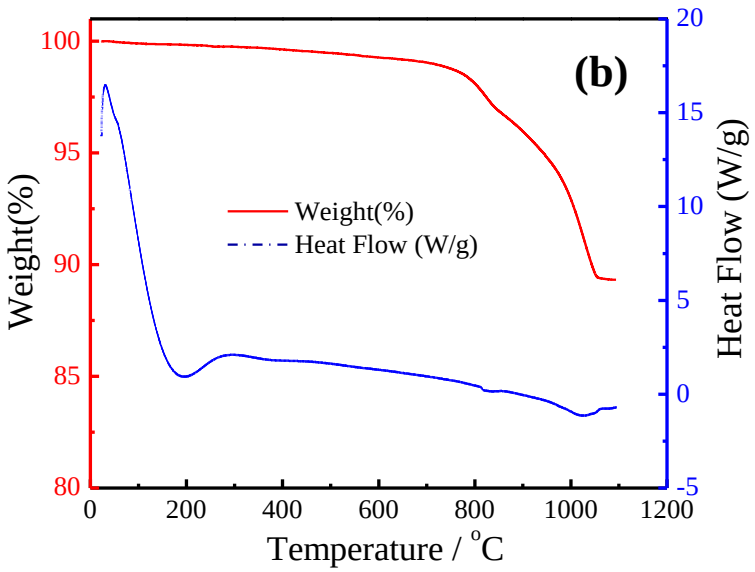

Figure 1. TGA-DSC plots of $BaCe_{0.9}Lu_{0.1}O_{3-\alpha}$ gel before (a) and after (b) ashing measurement.

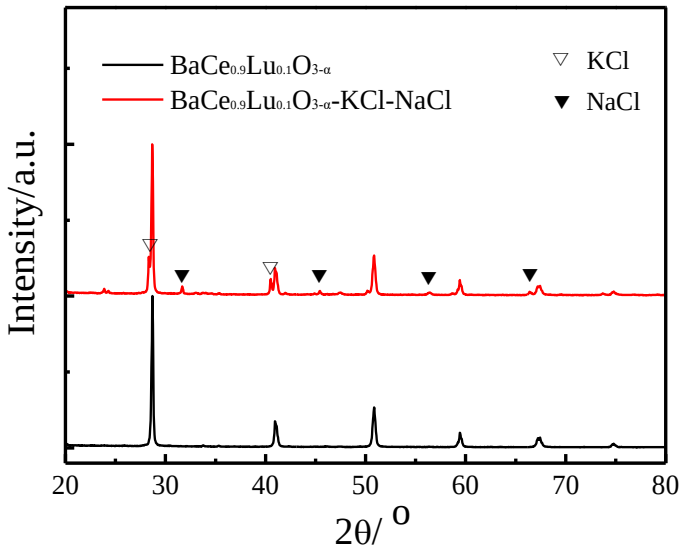

Figure 2. XRD patterns of $BaCe_{0.9}Lu_{0.1}O_{3-\alpha}$ and $BaCe_{0.9}Lu_{0.1}O_{3-\alpha}$-NaCl-KCl.

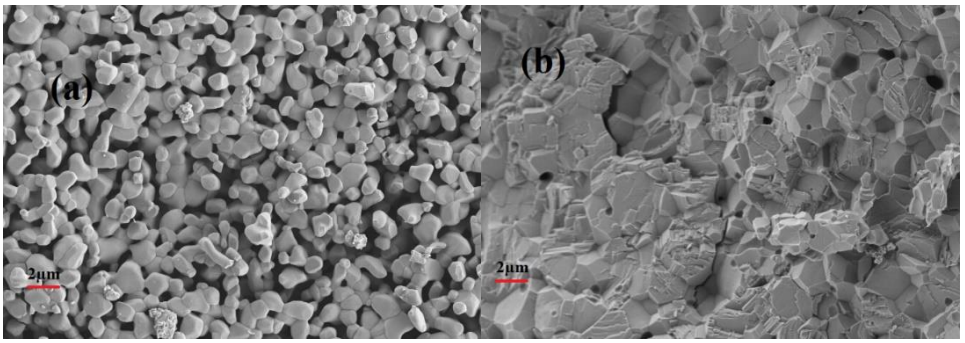

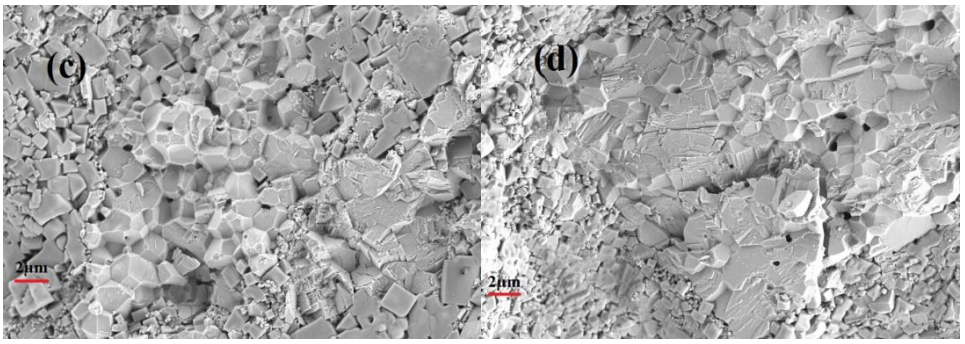

Figure 3. SEM photos of the morphologies of the external and cross-sectional surfaces of $BaCe_{0.9}Lu_{0.1}O_{3-\alpha}$ (a,b) and $BaCe_{0.9}Lu_{0.1}O_{3-\alpha}$-NaCl-KCl (c,d).

SEM photos of the morphologies of the external and cross-sectional surfaces of $BaCe_{0.9}Lu_{0.1}O_{3-\alpha}$ and $BaCe_{0.9}Lu_{0.1}O_{3-\alpha}$-NaCl-KCl are displayed in Fig. 3. From Fig. 3(a,b), the grain size is relatively uniform and the grain boundary is initially formed. In the Fig. 3(c,d) view, grains are obviously aggregated, and the bonding between grains is close. This may be due to NaCl-KCl in a molten state binding closely to $BaCe_{0.9}Lu_{0.1}O_{3-\alpha}$ at 750 °C. As can be seen from Fig. 3(c,d), there are still very few stomata, which are closed stomata after air tightness test, indicating that the gas will not pass through the sample naturally and will not affect the test [23–26].

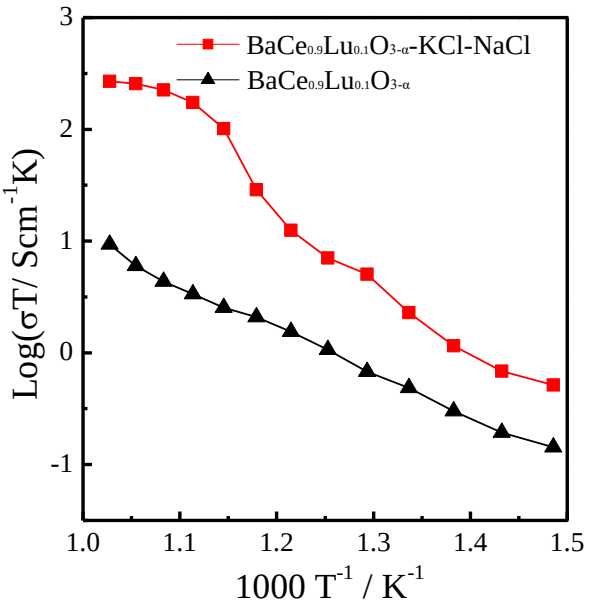

Figure 4. log (σT) ~ 1000 T^{-1} plots of $BaCe_{0.9}Lu_{0.1}O_{3-\alpha}$ and $BaCe_{0.9}Lu_{0.1}O_{3-\alpha}$-NaCl-KCl in dry nitrogen at 400–700 °C.

Fig. 4 shows the log (σT) ~ 1000 T^{-1} plots of $BaCe_{0.9}Lu_{0.1}O_{3-\alpha}$ and $BaCe_{0.9}Lu_{0.1}O_{3-\alpha}$-NaCl-KCl in dry nitrogen at 400–700 °C. For $BaCe_{0.9}Lu_{0.1}O_{3-\alpha}$, the relationship between abscissa 1000 T^{-1} and ordinate log (σT) in the Arrhenius curve is basically linear. The slope of $BaCe_{0.9}Lu_{0.1}O_{3-\alpha}$-NaCl-KCl is

smaller than that of $BaCe_{0.9}Lu_{0.1}O_{3-\alpha}$ at 600–700 °C, which indicates that the activation energy of the composite electrolyte decreases after NaCl-KCl becomes molten [24]. It can be seen from Fig. 4 that the values of conductivities increase gradually with the increase of temperature, and reach the maximum values at 700 °C. The highest conductivities of $BaCe_{0.9}Lu_{0.1}O_{3-\alpha}$ and $BaCe_{0.9}Lu_{0.1}O_{3-\alpha}$-NaCl-KCl are 9.5×10^{-2} S·cm^{-1} and 2.8×10^{-1} S·cm^{-1} at 700 °C, respectively [24–25].

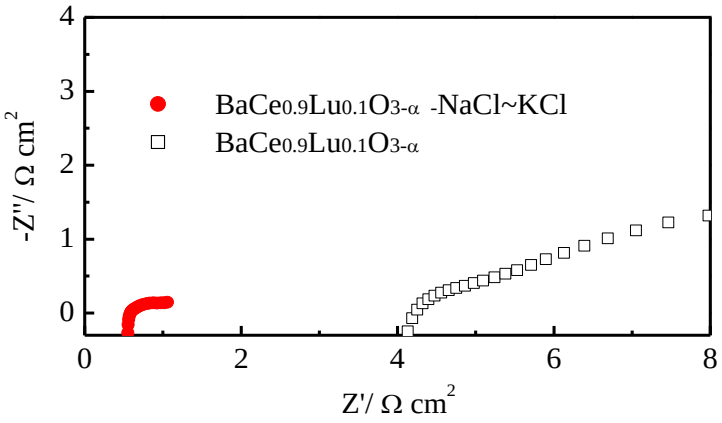

Figure 5. The AC impedance spectrogram of $BaCe_{0.9}Lu_{0.1}O_{3-\alpha}$ and $BaCe_{0.9}Lu_{0.1}O_{3-\alpha}$-NaCl-KCl under an open-circuit condition at 700 °C.

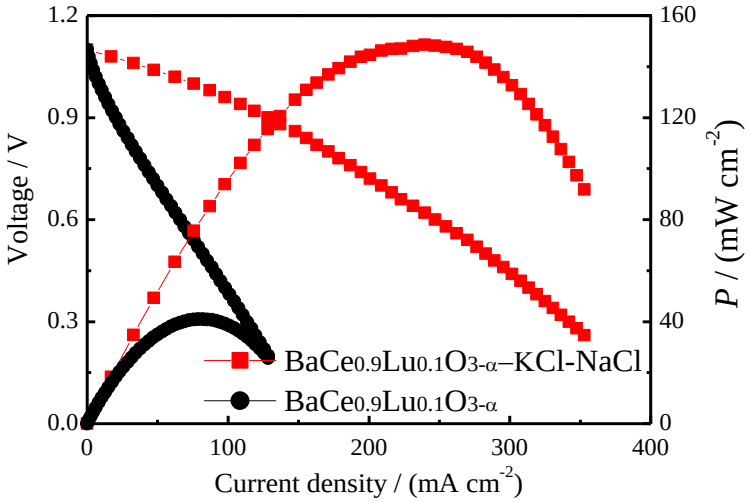

Figure 6. *I-V-P* curves of $BaCe_{0.9}Lu_{0.1}O_{3-\alpha}$ and $BaCe_{0.9}Lu_{0.1}O_{3-\alpha}$-NaCl-KCl at 700 °C.

The Fig. 5 shows the AC impedance spectrogram of $BaCe_{0.9}Lu_{0.1}O_{3-\alpha}$ and $BaCe_{0.9}Lu_{0.1}O_{3-\alpha}$-NaCl-KCl under an open-circuit condition measured at 700 °C. The intercept of the real axis usually represents the ohmic resistance (R_o) at high frequencies. The impedance spectra consist of a quarter-circle and a ray, which correspond to the ohmic resistance (R_o), total resistance (R_t) and electrolyte-electrode interface resistance from left to right, respectively. The difference between R_o and R_t on the

real axis is the polarization resistance (R_p). In Fig. 5, the R_p of $BaCe_{0.9}Lu_{0.1}O_{3-\alpha}$-NaCl-KCl (0.16 $\Omega \cdot cm^2$) is lower than that of $BaCe_{0.9}Lu_{0.1}O_{3-\alpha}$ (0.38 $\Omega \cdot cm^2$). The NaCl-KCl can not only greatly reduce the resistance but also enhance the fast transport capability of the composite electrolyte.

Fig. 6 is the discharge diagram of $BaCe_{0.9}Lu_{0.1}O_{3-\alpha}$ and $BaCe_{0.9}Lu_{0.1}O_{3-\alpha}$-NaCl-KCl at 700 °C. The initial open circuit voltages (OCVs) are 1.09 V, which indicate that the samples have good compactness. With the decrease of OCVs, current and power density increase correspondingly. When the current density of $BaCe_{0.9}Lu_{0.1}O_{3-\alpha}$-NaCl-KCl is 265 $mA \cdot cm^{-2}$, the maximum power density is 146 $mW \cdot cm^{-2}$ at 700 °C.

4. CONCLUSIONS

In this study, $BaCe_{0.9}Lu_{0.1}O_{3-\alpha}$ was prepared by the sol-gel method and $BaCe_{0.9}Lu_{0.1}O_{3-\alpha}$-NaCl-KCl was also synthesized using $BaCe_{0.9}Lu_{0.1}O_{3-\alpha}$ combined with sodium and potassium chloride. The XRD pattern of the sintered $BaCe_{0.9}Lu_{0.1}O_{3-\alpha}$ showed it is orthorhombic $BaCeO_3$ phase. SEM results indicated that NaCl-KCl in molten state binds closely to $BaCe_{0.9}Lu_{0.1}O_{3-\alpha}$ and the bonding between grains is close. The polarization resistances (R_p) of $BaCe_{0.9}Lu_{0.1}O_{3-\alpha}$ and $BaCe_{0.9}Lu_{0.1}O_{3-\alpha}$-NaCl-KCl are 0.38 $\Omega \cdot cm^2$ and 0.16 $\Omega \cdot cm^2$ under an open-circuit condition at 700 °C, respectively.

ACKNOWLEDGEMENTS
This work was supported by the National Natural Science Foundation (No. 51402052, 21602029) of China, The Natural Science Project of Anhui Province (No. KJ2018A0337), Excellent Youth Foundation of Anhui Educational Committee (No. gxyq2018046), The Guangdong Science and Technology Program (2017B030314002), Horizontal cooperation project of Fuyang municipal government and Fuyang Normal College (No. XDHX2016019, XDHXTD201704).

References

1. G. L. Liu, W. Liu Q. Kou and S. J. Xiao, *Int. J. Electrochem. Sci*., 13 (2018) 2641.
2. Y. Yang, H. Hao, L. Zhang, C. Chen, Z. Luo, Z. Liu, Z. Yao, M. Cao and H. Liu, *Ceram. Int.*, 44 (2018) 11109.
3. Y. N. Chen, T. Tian, Z. H. Wan, F. Wu, J. T. Tan and M. Pan, *Int. J. Electrochem. Sci.*, 13 (2018) 3827.
4. T. Hibino, K. Kobayashi, P. Lv, M. Nagao, S. Teranishi, and T. Mori, *J. Electrochem. Soc.*, 164 (2017) F557.
5. J. Luo, A.H. Jensen, N.R. Brooks, J. Sniekers, M. Knipper, D. Aili, Q. Li, B. Vanroy, M. Wübbenhorst, F. Yan, L.V. Meervelt, Z. Shao, J. Fang, Z.-H. Luo, D.E.D. Vos, K. Binnemans, and J. Fransaer, *Energy Environ. Sci.*, 8 (2015) 1276.
6. A.A. Solovyev, S.V. Rabotkin, A.V. Shipilova and I.V. Ionov, *Int. J. Electrochem. Sci*., 14 (2019) 575.
7. C. Xia, Z. Qiao, C. Feng, J. Kim, B. Wang and B. Zhu, *Materials*, 11(2018) 40.
8. Y. Tian, Z. Lü, X. Guo and P. Wu, *Int. J. Electrochem. Sci*., 14 (2019) 1093.
9. X. Fang, J. Zhu and Z. Lin, *Energies*. 11 (2018) 1735.
10. M. A. Haque, A. B. Sulong, E. H. Majlan, K. S. Loh, T. Husaini and R. Rosli, *Int. J. Electrochem.*

Sci., 14 (2019) 371.
11. Z. Zhang, L. Chen, Q. Li, T. Song, J. Su, B. Cai, H. He, *Solid State Ionic*s, 323 (2018) 25.
12. W. Wang, D. Medvedev and Z. Shao, *Adv. Funct. Mater.*, (2018) 1802592.
13. S.H. Morejudo, R. Zanón, S. Escolástico, I. Yuste-Tirados, H. Malerød-Fjeld, P.K. Vestre, W.G. Coors, A. Martínez, T. Norby, J.M. Serra and C. Kjølseth, *Science*, 353 (2016) 563.
14. E. Pikalova and D. Medvedev, *Int. J. Hydrogen Energ.*, 41 (2016) 4016.
15. S. Y. Bae, J.-Y. Park and H.-T. Lim, *Electrochim. Acta*, 236 (2017) 399.
16. J. Xiao, L. Chen, H. Yuan, L. Ji, C. Xiong, J. Ma and X. Zhu, *Mater. Lett.*, 189 (2017) 192.
17. J. Lyagaeva, G. Vdovin, L. Hakimova, D. Medvedev, A. Demin and P. Tsiakaras, *Electrochim. Acta*, 251 (2017) 554.
18. G. S. Reddy and R. Bauri, *J. Alloy Compd.*, 688 (2016) 1039.
19. J.M. Sailaja, K.V. Babu, N. Murali, and V. Veeraiah, *J. Adv. Res.*, 8 (2017) 169.
20. J. Song, B. Meng and X. Tan, *Ceram. Int.*, 42 (2016) 13278.
21. F. Liu, J. Dang, J. Hou, J. Qian, Z. Zhu, Z. Wang and W. Liu, *J. Alloy Compd.*, 639 (2015) 252.
22. K.-Y. Park, T.-H. Lee, S. Jo, J. Yang, S.-J. Song, H.-T. Lim, J.H. Kim and J.-Y. Park, *J. Power Sources*, 336 (2016) 437.
23. A.I.B. Rondao, S.G. Patricio, F.M.L. Figueiredo and F.M.B. Marques, *Int. J. Hydrogen Energ.*, 39 (2014) 5460.
24. N.C.T. Martins, S. Rajesh and F.M.B. Marques, *Mater. Res. Bull.*, 70 (2015) 449.
25. K.-Y. Park, T.-H. Lee, J.-T. Kim, N. Lee, Y. Seo, S.-J. Song and J.-Y. Park, *J. Alloy Compd.*, 585 (2014) 103.
26. Q. Guan, H. Wang, H. Miao, L. Sheng and H. Li, *Ceram. Int.*, 43 (2017) 9317.
27. R. Shi, J. Liu, H. Wang, F. Wu, H. Miao and Y. Cui, *Int. J. Electrochem. Sci.*, 12 (2017) 11594.
28. W. Zhang, M. Yuan, H. Wang and J. Liu, *J. Alloy Compd.*, 677(2016) 38.
29. R. Shi, J. Liu, H. Wang, F. Wu and H. Miao, *Ceram. Int.*, 43 (2017) 16931.
30. Q. Guan, H. Wang, H. Miao, L. Sheng and H. Li, *Ceram. Int.*, 43 (2017) 9317.
31. A. Matsuda, S. Oh, V.H. Nguyen, Y. Daiko, G. Kawamura and H. Muto, *Electrochim. Acta*, 56 (2011) 9364.
32. M.T. Soo, N. Prastomo, A. Matsuda, G. Kawamura, H. Muto, A.F.M. Noor, Z. Lockman and K.Y. Cheong, *Appl. Surf. Sci.*, 258 (2012) 5250.